

ODUSSEAS: Upgraded version with new reference scale and parameter determinations for 82 planet-host M dwarf stars in SWEET-Cat

A. Antoniadis-Karnavas^{1,2}, S. G. Sousa¹, E. Delgado-Mena¹, N. C. Santos^{1,2}, and D. T. Andreasen³

¹ Instituto de Astrofísica e Ciências do Espaço, Universidade do Porto, CAUP, Rua das Estrelas, 4150-762 Porto, Portugal
e-mail: alexandros.antoniadis@astro.up.pt

² Departamento de Física e Astronomia, Faculdade de Ciências, Universidade do Porto, Rua do Campo Alegre, 4169-007 Porto, Portugal

³ Independent Researcher

Received 14 May 2024 / Accepted 8 July 2024

ABSTRACT

Aims. Obtaining accurate derivations of stellar atmospheric parameters is crucial in the fields of stellar and exoplanet characterization. We present the upgraded version of our computational tool ODUSSEAS with a new reference scale applied to derive T_{eff} and $[\text{Fe}/\text{H}]$ values for M dwarfs.

Methods. The new reference dataset of ODUSSEAS consists of T_{eff} values based on interferometry, and $[\text{Fe}/\text{H}]$ values derived by applying updated values for the parallaxes. These reference parameters are related to the pseudo-equivalent widths (EWs) of more than 4000 stellar absorption lines. The machine learning Python "scikit learn" package creates models to determine the stellar parameters for subsequent analysis.

Results. We determined T_{eff} and $[\text{Fe}/\text{H}]$ values for 82 planet-host stars in SWEET-Cat. We demonstrate that our new version of ODUSSEAS is capable of determining the parameters with a greater accuracy than the original by comparing our results to other methods in literature. We also compared our parameters for the same stars by measuring their spectra obtained from several instruments, showing the consistency of our determinations with standard deviation of 30 K and 0.03 dex. Finally, we examined the correlation among planetary mass and stellar metallicity, confirming prior evidence indicating that massive planets mainly form around metal-rich stars in the case of M dwarfs as well.

Key words. methods: data analysis – techniques: spectroscopic – stars: atmospheres – stars: fundamental parameters – stars: late-type – planetary systems

1. Introduction

Accurate determinations of stellar parameters are essential for understanding the formation and evolution of stars. In the case of M dwarfs, which are the majority of stars in our Galaxy, their characterization is important to construct the dynamical and chemical evolution of the Galaxy (Lépine et al. 2007; Hejazi et al. 2020). In the fast-growing field of exoplanet detection and characterization, the stars influence the properties of the planets forming and orbiting around them as well as the measurement of their masses and radii (Everett et al. 2013; Martinez et al. 2019; Loaiza-Tacuri et al. 2023). Abundance determinations of the host stars are important to better understand the formation and evolution of planetary systems (Adibekyan et al. 2013; Ghezzi et al. 2021).

There are some difficulties that need to be overcome in the derivation of stellar atmospheric parameters for M dwarfs, such as effective temperature (T_{eff}) and metallicity (expressed as $[\text{Fe}/\text{H}]$). The spectroscopic study of M dwarfs is more complicated compared to that of FGK stars, because their molecules are the dominant sources of opacity (Woolf, & Wallerstein 2005), creating thousands of spectral lines that are poorly known and many of them blend with each other. Therefore, the position of the continuum is hardly identified in spectra of M dwarfs. A

common approach to derive the atmospheric parameters for FGK stars is by measuring the equivalent widths (EWs) of many metal lines, but in the case of M dwarfs, the measurements of pseudo-EWs have been used (Neves et al. 2012, 2014; Maldonado et al. 2015). Methods using spectral synthesis in the optical have not achieved as precise results as in FGK stars, because of the poor knowledge of many molecular line strengths. However, spectral synthesis in the near-infrared (NIR) has made progress, as shown by several studies (Önehag et al. 2012; Lindgren et al. 2016; Rajpurohit et al. 2018; Passegger et al. 2019). Due to the complexity of M dwarf spectra, most attempts to derive T_{eff} and $[\text{Fe}/\text{H}]$ have used photometric calibrations (Bonfils et al. 2005; Johnson & Apps 2009; Neves et al. 2012) or spectroscopic indices (Rojas-Ayala et al. 2010, 2012; Mann et al. 2013a). Uncertainties in $[\text{Fe}/\text{H}]$ vary from 0.20 dex using photometric calibrations to 0.10 dex using spectroscopic scales in the NIR (Rojas-Ayala et al. 2012). Regarding T_{eff} , precisions better than 100 K have been achieved, but determinations still suffer from uncertainties and systematic errors that range from 150 to 300 K (Casagrande et al. 2008; Rojas-Ayala et al. 2012). More accurate methods of determining M dwarf parameters could extend the knowledge and the input for improving the theoretical modeling of stars, which

in turn, would lead to an improved understanding and greater progress in stellar characterization.

Machine learning has become a very popular approach, with applications in many fields of science nowadays. The algorithms of machine learning methods receive input data and by applying statistical analysis they can predict output values accurately, without the need for the user to explicitly create a specific model beforehand. An overall review of the applications of machine learning to astrophysical problems can be found in Ball & Brunner (2010) and Ivezić et al. (2014). The interest of creating automatic processes with machine learning algorithms has begun to emerge from the vast volume of survey data (Howard 2017). Recently, in the field of stellar astronomy, machine learning methods have been applied to a vast series of problems such as the identification of symbiotic stars (Akras et al. 2019), the improvement of period-luminosity relations for variable stars (Ucci et al. 2019), and the determination of mass, age and distance for red-giant stars (Das & Sanders 2019). In particular, for the characterization of M dwarfs, apart from our original work (Antoniadis-Karnavas et al. 2020), Passegger et al. (2020) presented a deep neural network to analyze high-resolution stellar spectra and predict stellar atmospheric parameters. The convolutional network was trained on synthetic PHOENIX-ACES spectra in different optical and NIR wavelength regions.

Given the utility of machine learning techniques and the difficulty in obtaining parameters for M dwarfs, we developed a machine learning method useful for this kind of stars (Antoniadis-Karnavas et al. 2020). Our code, Observing Dwarfs Using Stellar Spectroscopic Energy-Absorption Shapes (ODUSSEAS¹), follows the pseudo-EW approach. It is based on a supervised machine learning algorithm, meaning that it is provided with both input and expected output and uses these to create a model. It makes use of the machine learning "scikit learn" package of Python and offers a quick automatic derivation of T_{eff} and $[\text{Fe}/\text{H}]$ for M dwarf stars using their 1D spectra and resolutions as input. The input to the machine learning function of ODUSSEAS are the values of precomputed pseudo-EWs for a set of HARPS GTO spectra and the expected output are the values of their reference T_{eff} and $[\text{Fe}/\text{H}]$ from selected literature studies, respectively. In the original version of the tool, the reference values of T_{eff} came from Casagrande et al. (2008), following the IRFM method as modified for M dwarfs, and the reference values of $[\text{Fe}/\text{H}]$ came from Neves et al. (2012), for a dataset of 65 stars.

After the publication of the tool, part of our team participated to a comparative study of methods for determination in the work by Passegger et al. (2022). In that study, stellar atmospheric parameters of 18 well-studied M dwarfs observed with the CARMENES spectrograph were determined following different approaches. Four different methods were applied to the spectra: two of them, Pass-19 code (Passegger et al. 2018, 2019) and SteparSyn (Tabernero et al. 2021), are based on synthetic spectra fitting; while the other two, deep learning (Passegger et al. 2020) and ODUSSEAS (Antoniadis-Karnavas et al. 2020), are based on the machine learning concept. In that work, the discrepancies in the derived stellar parameters were analyzed in several analysis runs. The goal was to minimize these discrepancies and find stellar parameters that would be more consistent with the literature value. Similarly to the comparison of the reference T_{eff} , with values by Mann et al. (2015) as showed in Antoniadis-Karnavas et al. (2020), it was noticed that the photometric reference scale of ODUSSEAS gave results underestimated, compared to the other three methods, as well as to the

literature values. The mean differences of the ODUSSEAS results were: -86 K to the literature median, -123 K to the interferometric literature values, -178 K to Pass-18 code, -132 K to SteparSyn, and -176 K to deep learning, respectively. From these comparisons, it was clear that the IRFM/MOITE-based photometric reference scale was consistently underestimating T_{eff} values for M dwarfs. Thus, we examined the possibility of replacing our photometric reference dataset with the reference values from interferometry as a potential improvement of our determinations.

2. Upgrade with new reference scale

To tackle the problem presented in (Passegger et al. 2022), we searched the literature to find T_{eff} values based on interferometry for a sufficient number of stars among the 110 we already had HARPS GTO spectra for.

One year after the publication of ODUSSEAS (Antoniadis-Karnavas et al. 2020), Khata et al. (2021) presented a sample of 23 target stars with high precision long-baseline interferometric measurements of radii (Boyajian et al. 2012; Mann et al. 2015; Rabus et al. 2019) for the calibration of stellar parameters. In that work, 13 calibrators were chosen from Newton et al. (2015) where the bolometric luminosities were measured from multi-color photometry (Boyajian et al. 2012) and T_{eff} were calculated using the interferometric radius and bolometric flux (Mann et al. 2013b). They supplemented this calibration sample with 6 M dwarfs taken from Mann et al. (2015), where the bolometric flux was calculated by integrating over the radiative flux density and T_{eff} was calculated by fitting the optical spectra with the PHOENIX (BT-Settl) models (Allard et al. 2013). They also added four calibrators from Rabus et al. (2019), where the bolometric flux was estimated using PHOENIX models (Husser et al. 2013), along with photometric observations and T_{eff} was estimated using the Stefan-Boltzmann law. Khata et al. (2021) proceeded to a calibration, deriving stellar parameters for 271 stars. We had HARPS GTO spectra available for 43 of those 271 stars. Moreover, we increased our new reference dataset by adding 4 more stars from the HARPS GTO sample, with values derived by Rabus et al. (2019). Rabus et al. (2019) reported on 13 new high-precision measurements of stellar diameters for low-mass dwarfs obtained by means of NIR long-baseline interferometry with PIONIER at the Very Large Telescope Interferometer (VLTI). Together with accurate parallaxes from Gaia DR2, these measurements provided precise estimates for their linear radii, T_{eff} , masses, and luminosities. Thus, ODUSSEAS was upgraded by implementing a new reference dataset of 47 stars with T_{eff} based on interferometry (Khata et al. 2021; Rabus et al. 2019).

For these 47 stars, we derived $[\text{Fe}/\text{H}]$ values using the same method as in the original reference dataset, by applying the following relation from Neves et al. (2012):

$$[Fe/H] = 0.57\Delta(V - K_s) - 0.17. \quad (1)$$

Here, $\Delta(V - K_s) = (V - K_s)_{\text{obs}} - (V - K_s)_{\text{iso}}$, whereby $(V - K_s)_{\text{obs}}$ is the observed $V - K$ color and $(V - K_s)_{\text{iso}}$ is a fifth-order polynomial function of the absolute magnitude, M_{K_s} , with the coefficients being in increasing order: (51.1413, -39.3756, 12.2862, -1.83916, 0.134266, -0.00382023). As input values to the equation, we used the V and K magnitudes reported in Simbad² and the updated values of parallaxes from Gaia eDR3 (Gaia Collaboration 2020) for the calculation of M_{K_s} .

¹ <https://github.com/AlexandrosAntoniadis/ODUSSEAS>

² <http://simbad.cds.unistra.fr/simbad/>

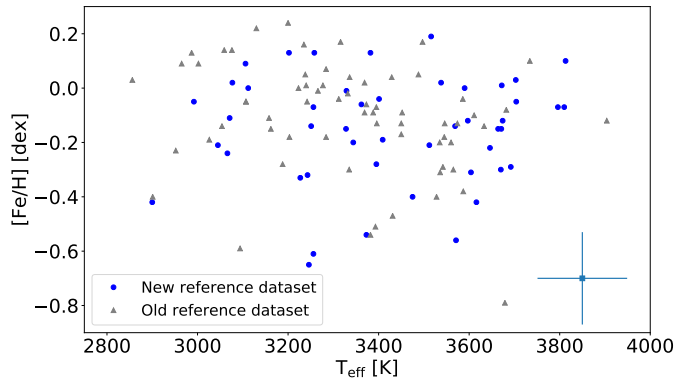


Fig. 1. Distribution of the new reference dataset (blue circles) in comparison to the old one (grey triangles). The cross symbol represents the uncertainties of the new reference T_{eff} and $[\text{Fe}/\text{H}]$, which are 99 K and 0.17 dex, respectively.

The new reference dataset is presented in Table A.1. The methods of derivation for the new reference values have intrinsic uncertainties of 99 K for T_{eff} and 0.17 dex for $[\text{Fe}/\text{H}]$, from Khata et al. (2021) and Neves et al. (2012), respectively. The distribution of the new reference dataset is presented in Fig 1, compared to the old one. The new reference values range from 2900 to 3813 K for T_{eff} and from -0.65 to 0.19 dex for $[\text{Fe}/\text{H}]$. The histograms of the new reference dataset, compared to the old one, are presented in Fig 2. The parameter space of applicability can be considered to range from 2700 to 4000 K for T_{eff} and from -0.82 to 0.24 dex for $[\text{Fe}/\text{H}]$. We have tested the new reference dataset on stars with parameters around these extreme values and we obtained accurate determinations with similar levels of precision to those of determinations that are inside the range of the reference parameters. The tool can operate beyond the strict range of reference parameters, as its machine learning models extrapolate reliably to the limits mentioned above.

Among the 37 stars in common across both reference datasets, the average difference between the new reference and the old reference scale is 151 K for T_{eff} and -0.01 dex for $[\text{Fe}/\text{H}]$. As we present and discuss below, these average differences between the reference datasets translate to average differences of the same order in the determinations for several samples of stars. Users can select (in the options) the scale whose reference dataset will then be applied in determining the parameters.

Similar steps as those applied to the original reference dataset presented by Antoniadis-Karnavas et al. (2020), were followed again, in order to check the machine learning efficiency, accuracy, and precision with this new reference dataset. Since our new reference dataset consists of fewer stars (47) than the original one (65), we decided to increase the percentage of stars in the training group from 70% to 80%, in order to include a relatively greater number of stars in the process of building the machine learning models, while still keeping a sufficient number of stars (10) for testing the predictions and measuring the mean absolute errors of the new models.

Again, we calculated the machine-learning regression metrics of "explained variance" (E.V.) and "r2" scores, as well as the mean absolute errors of the models, for our new reference dataset. The E.V. score varies mostly between 0.89 and 0.90, while the r2 score is between 0.88 and 0.89. These values are slightly lower than the respective scores between 0.92 and 0.94 of the original reference dataset, because the new population of reference stars is smaller than the initial one (47 compared to 65

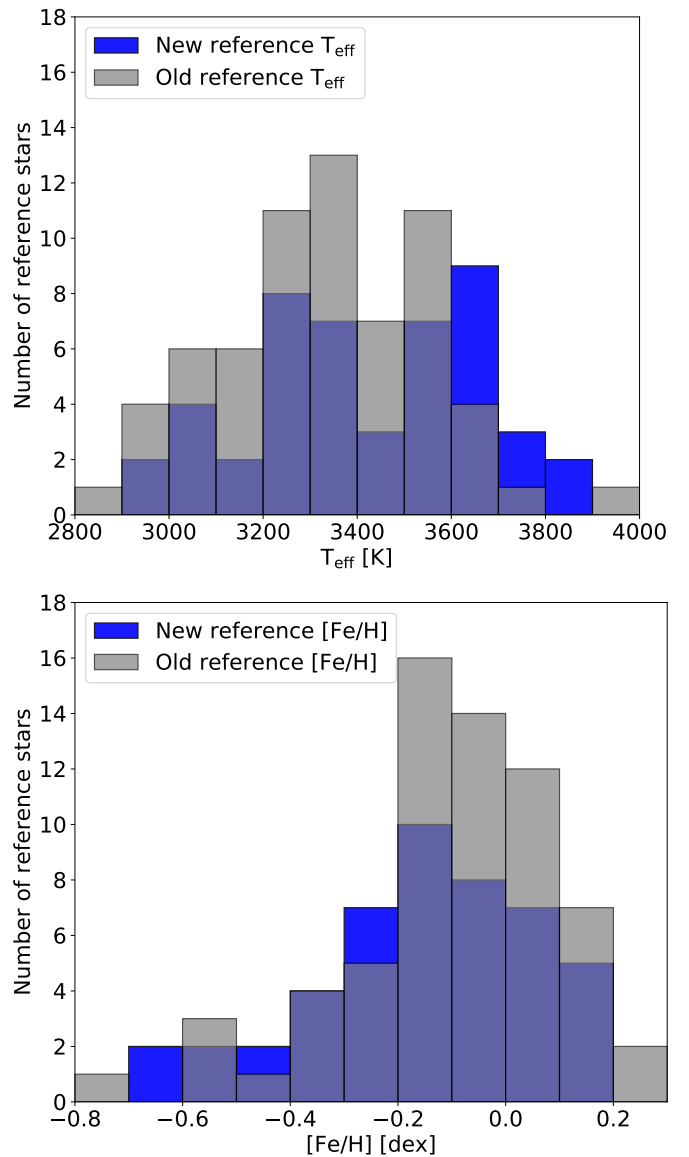


Fig. 2. Histograms for T_{eff} (upper panel) and $[\text{Fe}/\text{H}]$ (lower panel) of the new (blue) and old (grey) reference datasets.

stars). Still, the new scores are quite high for making predictions with sufficient accuracy and precision regarding M dwarfs.

The mean absolute errors of the machine learning models are around 65 K for T_{eff} and 0.04 dex for $[\text{Fe}/\text{H}]$ for all resolutions. Compared to the model errors of the original reference dataset (around 30 K and 0.04 dex, respectively), the precision of T_{eff} with the new reference dataset is lower, but still within the typical uncertainties of M dwarfs. However, most importantly, the accuracy of the T_{eff} determinations with the new reference dataset is greater, being in closer agreement with several other methods in literature, as shown later in Sect. 5.

Similarly to Antoniadis-Karnavas et al. (2020), we examined the parameter determination, model errors and dispersion for stars with spectra of different spectrographs comparing the results to their reference values as defined by the new reference dataset. These results are presented in Table 1. The predictions of ODUSSEAS had differences varying from 5 to 64 K for T_{eff} and from 0.00 to 0.05 dex for $[\text{Fe}/\text{H}]$ compared to the expected values. We also injected the intrinsic uncertainties of our new reference values to the new training datasets, as in Antoniadis-

Karnavas et al. (2020). These are 99 K for T_{eff} and 0.17 dex for [Fe/H], as reported by Khata et al. (2021) and Neves et al. (2012), respectively. We created Gaussian distributions on the parameters for each HARPS training dataset by perturbing their values according to their uncertainties. They lead to machine learning model errors varying from 90 to 99 K for T_{eff} and from 0.11 to 0.13 dex for [Fe/H], as the resolution of the spectra becomes lower. The predictions of the parameters remained within these error ranges compared to the expected reference values. These results take the intrinsic uncertainties into consideration and are presented in Table 2.

3. Application to ESPRESSO data of the highest resolution

After the analysis of the efficiency towards lower resolutions and the successful application to the spectrographs mentioned above, the tool has been also applied successfully on spectra from ESPRESSO³ (Pepe et al. 2021) spectrograph, that were made available to us. This case is special because the high resolution (HR=140000) and ultra-high resolution (UHR=190000) of ESPRESSO spectra are higher than the resolution (R=115000) of the HARPS reference spectra. For these very high resolutions of ESPRESSO and HARPS, the results derived by ODUSSEAS are essentially the same when using either directly the original higher-resolution spectra of ESPRESSO that are to be analyzed according to the HARPS reference spectra or by degrading them first to the lower (but still high) resolution of HARPS before being analyzed. Between the two procedures, the typical differences in the resulting parameters are smaller than the mean errors of our machine learning models. Therefore, we can analyze the original ESPRESSO spectra, as the process is less time-consuming than analyzing the respective degraded spectra and will still be able to determine their parameters with the same accuracy and precision. Studies that have used ODUSSEAS tool on ESPRESSO spectra have been already published for the M dwarfs LHS1140 (Lillo-Box et al. 2020), L98-59A (Demangeon et al. 2021), and TOI-3235 (Hobson et al. 2023), applying the original reference dataset, as well as for TOI-244 (Castro-González et al. 2023), applying the new reference dataset.

4. Determination of parameters for 82 planet-host stars in SWEET-Cat

The Catalogue of Stars With Exoplanets (SWEET-Cat⁴) contains planet-host stars and their parameters. It was originally introduced in (Santos et al. 2013). Since then, many more exoplanets have been confirmed, thereby significantly increasing the number of host stars listed there (Sousa et al. 2021). A crucial step for a comprehensive analysis of the exoplanets is the accurate and precise characterization of their host stars. Stellar parameters derived from high-resolution and high-S/N spectra can provide updated and precise parameters for the discovered planets. Statistical studies of exoplanets and their host stars require consistent measurements in order to avoid different systematics affecting the results. SWEET-Cat aims to provide stellar parameters in a consistent and homogeneous way, by analyzing high-quality spectra which are assembled for stars hosting planets.

In this work, we have determined T_{eff} and [Fe/H] values for 82 stars of SWEET-Cat. Among the planet-host stars in the cur-

rent SWEET-Cat archive, we searched for the stars with T_{eff} lower than 4000 K and G magnitude brighter than 13. The ESO archive⁵ is a main source of reduced spectral public data for SWEET-Cat. We searched the required data in the ESO archive using the "astroquery.eso" module and we downloaded data from the HARPS, ESPRESSO, UVES, and FEROS spectrographs. In most cases we downloaded more than one spectrum per star to achieve a higher S/N by combining them. We discarded spectra with S/N below 20, due to their bad quality. We co-added spectra until we reached a maximum S/N of 2000 for the combined spectrum. We obtained the final combined spectrum for each star for a given instrument by shifting all spectra to the same wavelength reference before the flux co-addition, using a cross-correlation function with the highest S/N individual spectrum taken as the mask. We used a sigma clipping to remove unusual peaks. We saved the final spectra in 1D fits-file format. On top of the ESO archive, we did the same process to collect spectra for more planet-host M dwarfs in SWEET-Cat, using the HARPS-N spectrograph (archived in the IA2⁶, Italian Center for Astronomical Archive), the SOPHIE⁷ spectrograph and the public archive of CARMENES⁸ spectrograph.

For some stars, we have co-added spectra from more than one instrument. We determined parameters for spectra from all the instruments to check the consistency of ODUSSEAS when using different instrumental data. For the next steps of our work, we selected those parameter values with the lowest estimated errors, instead of the average values, because the average can still be significantly affected by the presence of lower-quality spectra. The distribution of S/N values for the co-added spectra with the selected parameters and their correlation with the G magnitudes of the stars are presented in Fig. 3. The lowest S/N value in our spectra is 20, equal to the minimum value for which ODUSSEAS can provide reliable results (Antoniadis-Karnavas et al. 2020). The stars and their parameters, determined with both the new and the old reference datasets, are reported in Table B.1. The total error budgets are reported for each star individually. These are derived automatically when running ODUSSEAS, by adding quadratically the dispersion of the resulting stellar parameters and the maximum errors of the machine learning models at the respective resolution, after having taken into consideration the intrinsic uncertainties of the reference dataset during the machine learning process. In Fig. 4 we show the differences of the derived parameters for spectra of the same stars observed with different instruments. The differences are calculated compared to the average value from the multiple spectra as measured applying the new reference dataset. The values are quite consistent when ODUSSEAS is applied to different instruments. The standard deviation of the parameters, relative to the average values, is 30 K for T_{eff} and 0.03 dex for [Fe/H]. There are some large individual differences, but they are within the uncertainties reported.

The comparisons of selected determinations for all stars between the applications of the two reference datasets are presented in Fig. 5. There is an average difference of 138 K with standard deviation of 68 K between measurements occurring from the new and the old reference dataset. This value of difference is what we expected, based on the differences reported in the comparative study of different methods (Passegger et al.

⁵ http://archive.eso.org/wdb/wdb/adp/phase3_main/form

⁶ <http://archives.ia2.inaf.it/tng/>

⁷ <http://atlas.obs-hp.fr/sophie/>

⁸ <http://carmenes.cab.inta-csic.es/gto/jsp/reinserteral2017.jsp>

³ <https://www.eso.org/sci/facilities/paranal/instruments/espreso.html>

⁴ <https://sweetcat.iaastro.pt/>

Table 1. Machine learning (M.L.) results of T_{eff} and $[\text{Fe}/\text{H}]$, their dispersion (Disp.), the mean absolute errors (M.A.E.) of the models, and the reference values (Ref.) by applying the new reference scale.

Star	Spec.	Ref. T_{eff} [K]	M.L. T_{eff} [K]	M.A.E. T_{eff} [K]	Disp. T_{eff} [K]	Ref. [Fe/H] [dex]	M.L. [Fe/H] [dex]	M.A.E. [Fe/H] [dex]	Disp. [Fe/H] [dex]
Gl643	HARPS	3243	3238	65	11	-0.32	-0.31	0.04	0.01
Gl846	UVES	3810	3802	65	21	-0.07	-0.06	0.04	0.02
Gl514	CARMENES	3671	3624	65	33	-0.15	-0.15	0.04	0.03
Gl908	SOPHIE	3475	3507	65	53	-0.40	-0.36	0.04	0.03
Gl674	FEROS	3409	3473	65	42	-0.19	-0.14	0.04	0.03

Table 2. Machine learning (M.L.) results of T_{eff} and $[\text{Fe}/\text{H}]$ after injecting uncertainties with Gaussian distributions of 99 K and 0.17 dex in the parameters of the new training HARPS datasets, their dispersion (Disp.), the mean absolute errors (M.A.E.) of the models, and the reference values (Ref.) for comparison.

Star	Spec.	Ref. T_{eff} [K]	M.L. T_{eff} [K]	M.A.E. T_{eff} [K]	Disp. T_{eff} [K]	Ref. [Fe/H] [dex]	M.L. [Fe/H] [dex]	M.A.E. [Fe/H] [dex]	Disp. [Fe/H] [dex]
Gl643	HARPS	3243	3227	90	95	-0.32	-0.31	0.11	0.13
Gl846	UVES	3810	3794	92	107	-0.07	-0.11	0.11	0.18
Gl514	CARMENES	3671	3625	95	127	-0.15	-0.12	0.12	0.23
Gl908	SOPHIE	3475	3502	97	130	-0.40	-0.37	0.13	0.23
Gl674	FEROS	3409	3481	99	149	-0.19	-0.16	0.13	0.24

2022) when we had used the original reference dataset. Thus, the new interferometry-based T_{eff} scale compensates the under-estimation of the order of 140 K that was noticed and explained in Sect. 1. It seems to provide indeed more accurate values compared to the ones derived by the old reference scale, which is based on the IRFM method. Regarding the $[\text{Fe}/\text{H}]$ results in the lower panel, a small trend in differences is noticed for the metal-poor stars, which have slightly lower values with the new reference dataset. On the other hand, stars with $[\text{Fe}/\text{H}]$ results close to solar values and above appear to have either higher or lower values with the new reference dataset. These differences may occur due to the different samples of reference stars between the two datasets. Another reason may be the updated parallax values that are used to derive the reference $[\text{Fe}/\text{H}]$ in the new scale, which originate from Gaia eDR3, compared to the parallax values from Hipparcos that were used in the calculation of $[\text{Fe}/\text{H}]$ by Neves et al. (2012) in the initial reference dataset. Among the common stars in the two reference datasets, the new reference $[\text{Fe}/\text{H}]$ scale has an average difference of -0.01 dex with standard deviation of 0.02 dex compared to the initial one. The average difference in our results, applying the two reference datasets, is 0.00 dex with standard deviation of 0.05 dex. Having color-coded the datapoints of each panel with the values of the other parameter, looking at the T_{eff} differences in the upper panel, we notice that the extremely metal-poor stars of the sample tend to have comparatively smaller differences between the two reference scales (from 50 K to 150 K difference), rather than the stars with $[\text{Fe}/\text{H}]$ close to solar values and above, for which most of the differences are mainly from 150 K up to 300 K. In any case, users now have the option to set which reference version is meant to be applied for parameter determinations.

5. Comparison of results with literature studies

Having determined the parameters for the 82 M dwarfs, we proceeded to perform a comparison of our results (derived by applying the new reference dataset) with studies in the literature, with which we shared a sufficient amount of common stars (at least 15% of our sample) to ensure that the overall differences are of statistical significance. Thus, we selected four publications, with at least 13 stars in common each of them, in order to compare the determinations of T_{eff} and $[\text{Fe}/\text{H}]$. Maldonado et al. (2015) and Rojas-Ayala et al. (2012) derived the stellar parameters applying the concept of pseudo-EWs, while Passegger et al. (2018) and Mann et al. (2015) used spectral synthesis with PHOENIX models. The differences of parameters for stars in common are presented in Fig. 6.

Maldonado et al. (2015) used 112 ratios of pseudo-EWs of spectral features as a temperature diagnostic. The sample of 21 M dwarfs from Boyajian et al. (2012), with T_{eff} obtained from interferometric estimates of their radii, were used as calibrators. Combinations of features and ratios of features were used to derive calibrations for the determination of $[\text{Fe}/\text{H}]$. They assembled a list of 47 metallicity calibrators with available HARPS spectra, known parallaxes and magnitudes by using the photometric calibration provided by Neves et al. (2012). Regarding T_{eff} , the mean and median differences are -22 K and 0 K, respectively, with a standard deviation of 58 K. There seems to be a positive trend, as for cooler stars our determinations give slightly lower T_{eff} values and vice versa. The $[\text{Fe}/\text{H}]$ mean and median differences are small too, reasonably since both methods have used the relation by Neves et al. (2012) in their respective calibration processes for the determination of $[\text{Fe}/\text{H}]$. They are equal to -0.04 and -0.05, respectively, with a standard deviation of 0.05 dex.

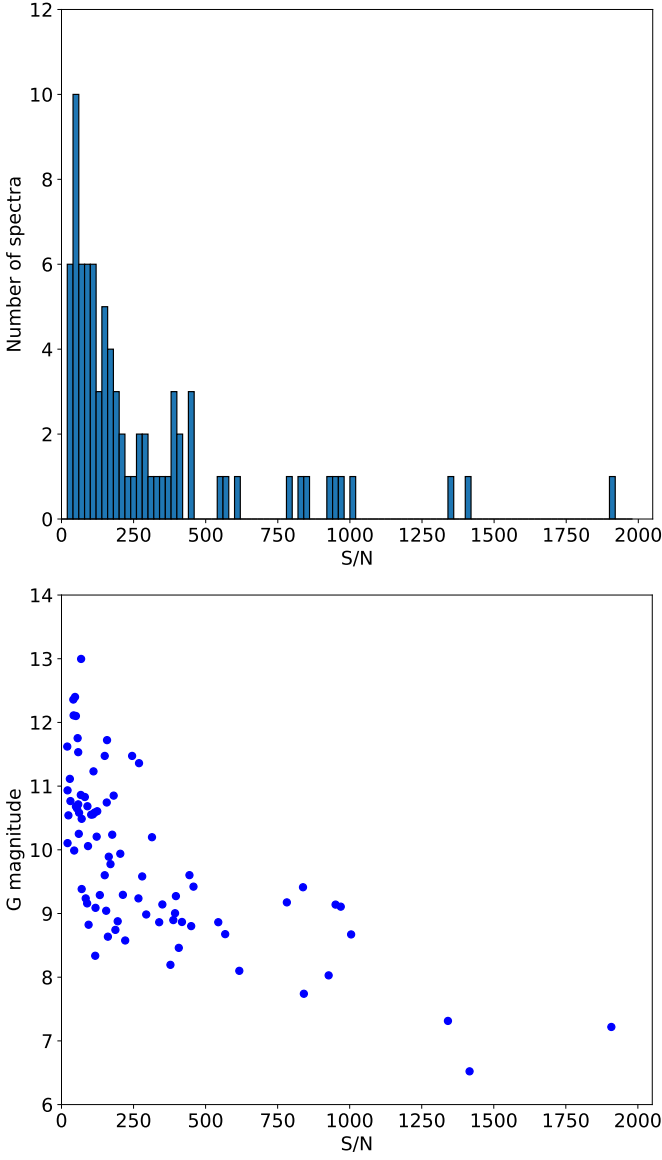


Fig. 3. Distribution of S/N values (upper panel) and their relation to the G magnitude (lower panel) for spectra of the 82 stars in SWEET-Cat.

Rojas-Ayala et al. (2012) measured the EWs of the Ca and Na lines, along with the spectral index quantifying the absorption due to H_2O opacity (the H_2O -K2 index). They set a pseudo-continuum for each feature, which is estimated from a linear fit to the median flux within $0.003 \mu\text{m}$ wide regions centered on the continuum points. Using empirical spectral type standards and synthetic models, they calibrated the H_2O -K2 index as an indicator of M dwarf spectral type and T_{eff} . They also presented a relationship that estimates the $[\text{Fe}/\text{H}]$ and $[\text{M}/\text{H}]$ metallicities of M dwarfs from their NaI, CaI, and H_2O -K2 measurements. Regarding T_{eff} , the mean and median differences are -66 K and -40 K, respectively, with a standard deviation of 97 K. $[\text{Fe}/\text{H}]$ mean and median differences are -0.11 and -0.12 dex, respectively, similar to our uncertainty range which varies between 0.11 and 0.14 dex. The standard deviation of the $[\text{Fe}/\text{H}]$ difference is 0.12 dex.

Passegger et al. (2018) adapted the method described in Passegger et al. (2016), which determined T_{eff} , $\log g$, and $[\text{Fe}/\text{H}]$ using the grid of PHOENIX model spectra presented by Husser et al. (2013). The PHOENIX-ACES model grid they used was

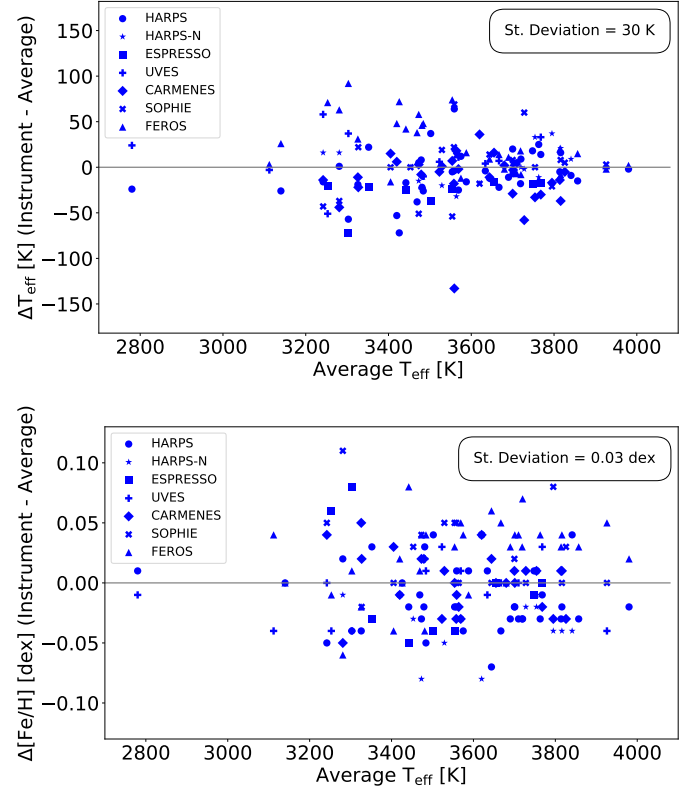


Fig. 4. Comparison of determinations for stars with spectra from different instruments. The differences are relative to the average values of T_{eff} (upper panel) and $[\text{Fe}/\text{H}]$ (lower panel).

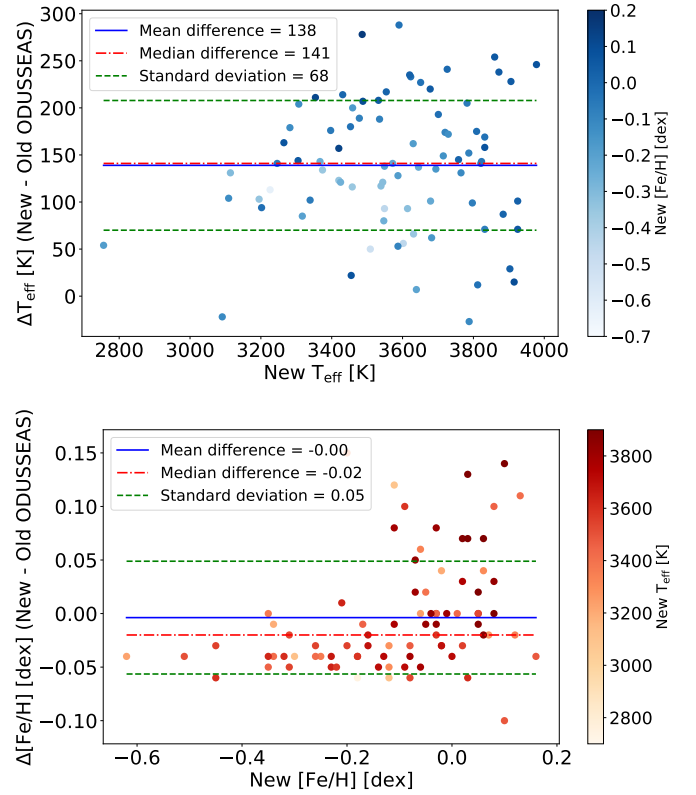


Fig. 5. T_{eff} comparison (upper panel) and $[\text{Fe}/\text{H}]$ comparison (lower panel) for 82 stars in SWEET-Cat by applying the new and the old reference datasets.

especially designed for modeling the spectra of cool dwarfs, because it uses a new equation of state to improve the calculations of molecule formation in cool stellar atmospheres. They applied a χ^2 method to derive the stellar parameters by fitting the models to high-resolution spectroscopic data. Regarding T_{eff} , the mean and median differences are -50 K and -45 K, respectively, with a standard deviation of 48 K. The [Fe/H] mean and median differences are -0.09 and -0.12 dex, respectively, similar to the typical uncertainty range of our measurements. The standard deviation of the [Fe/H] difference is 0.12 dex. There seems to be a positive trend, as for stars with low metallicity, our determinations give lower [Fe/H] values, while for higher-metallicity stars, the differences become generally smaller.

Mann et al. (2015) calculated T_{eff} by comparing optical spectra with the CFIST suite of the BT-SETTL version of the PHOENIX atmosphere models (Allard et al. 2013). Metallicities were calculated from the NIR spectra using the empirical relations from Mann et al. (2013a) for K7–M4.5 dwarfs and from Mann et al. (2014) for M4.5–M7 dwarfs. These studies provide relations between the EWs of atomic features such as Na and Ca in NIR spectra and the metallicity of the star, calibrated using wide binaries with an FGK primary and an M dwarf companion. Regarding T_{eff} , the mean and median differences are -11 and -4 K, respectively, with a standard deviation of 31 K. The [Fe/H] mean and median differences are -0.11 and -0.10 dex, respectively, within the typical uncertainty range of our measurements. The standard deviation of the [Fe/H] difference is 0.07 dex.

In all four cases, generally our T_{eff} values are slightly lower with average differences that are much smaller than the error range of our determinations, which is mostly slightly above 90 K. Regarding [Fe/H], the difference with Maldonado et al. (2015) is considerably small since both methods use, as their calibration scale, the relation by Neves et al. (2012); however, this relation was then applied to different set of reference stars and with different values of parallaxes. Comparing our [Fe/H] results with the other three methods, we notice that our determinations are on average -0.11 dex lower; that is, exactly as the common error range of our determinations after having taken into account the intrinsic reference uncertainties in our final error estimation.

Furthermore, in Fig. 7, we present the differences between our parameters derived with the new reference dataset of ODUSSEAS and the previously reported parameters in SWEET-Cat. As non-homogeneous parameters, represented with blue circles, we consider those parameters that were listed in SWEET-Cat from different studies in literature following various methods. As the old homogeneous parameters, represented with red triangles, we consider the parameters that were derived based on the scales of Casagrande et al. (2008) and Neves et al. (2012), which are the old reference scales of ODUSSEAS as well. The mean and median differences, as well as the standard deviation, regarding the comparisons between our new results and the parameters from all the sources examined above, are summarized in Table 3.

6. Planetary mass-stellar metallicity correlation

Theory of planet formation suggests correlation between the presence of giant planets and the high metallicity of their host stars (Laughlin 2000; Gonzalez et al. 2001). Santos et al. (2003, 2004) confirmed that the frequency of planets is a rising function of the stellar metallicity, at least for stars with [Fe/H] > 0. Fischer & Valenti (2005) also concluded that above solar metallicity, there is a smooth and rapid rise in the fraction of stars with planets. Furthermore, in that study, high stellar metallic-

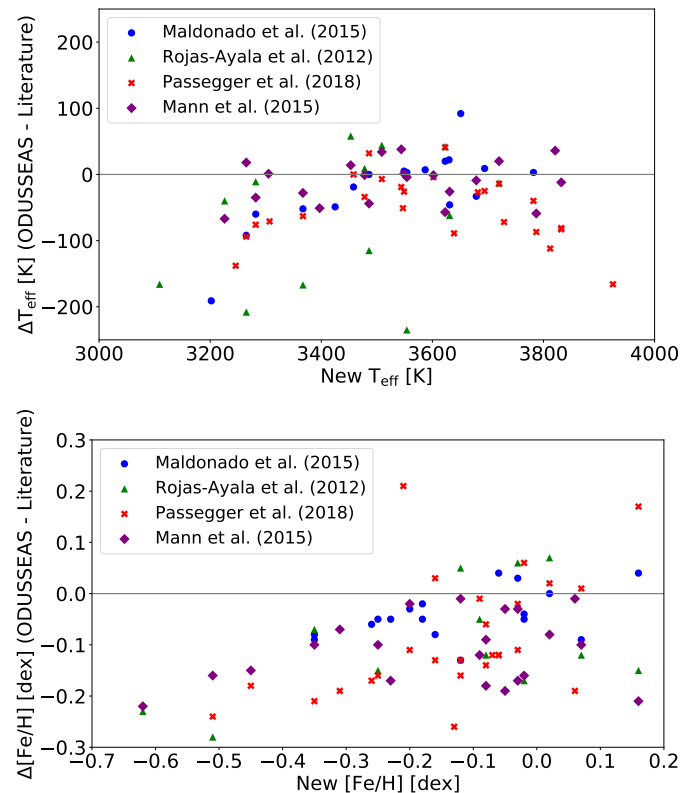


Fig. 6. T_{eff} comparison (upper panel) and [Fe/H] comparison (lower panel) between our results and studies in the literature for stars in common.

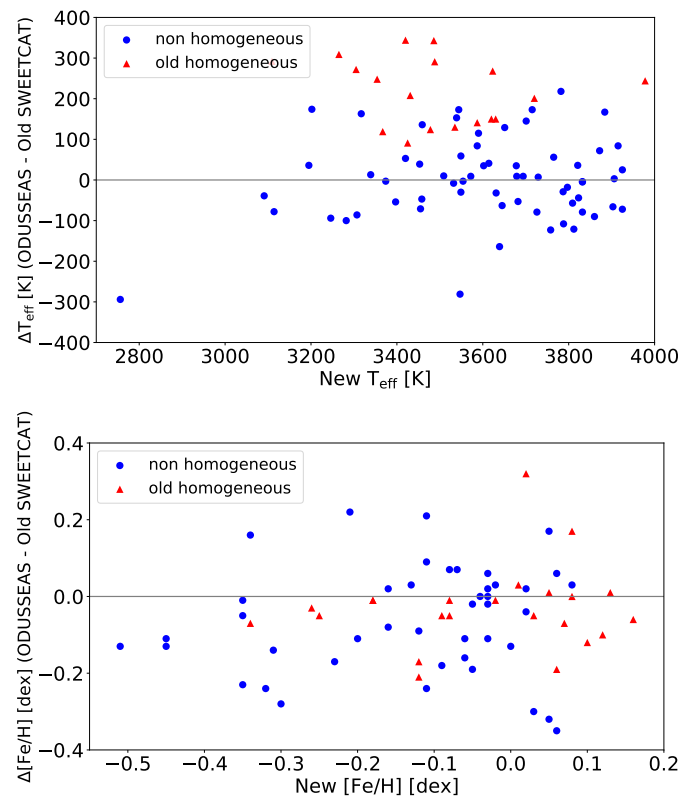


Fig. 7. T_{eff} comparison (upper panel) and [Fe/H] comparison (lower panel) between our new results and previous results reported in SWEET-Cat.

Table 3. Mean, median, and standard deviation of differences between our new results applying ODUSSEAS and literature studies.

Source	Mean ΔT_{eff} [K]	Median ΔT_{eff} [K]	St.D. ΔT_{eff} [K]	Mean $\Delta[\text{Fe}/\text{H}]$ [dex]	Median $\Delta[\text{Fe}/\text{H}]$ [dex]	St.D. $\Delta[\text{Fe}/\text{H}]$ [dex]
Maldonado et al.(2015)	-22	0	58	-0.04	-0.05	0.05
Rojas-Ayala et al. (2012)	-66	-40	97	-0.11	-0.12	0.12
Passegger et al. (2018)	-50	-45	48	-0.09	-0.12	0.12
Mann et al. (2015)	-11	-4	31	-0.11	-0.10	0.07
Non Hom. Sweet-Cat	1	-3	101	-0.06	-0.05	0.14
Old Hom. Sweet-Cat	218	226	80	-0.03	-0.05	0.11

ity appears to be correlated with the presence of multiple-planet systems and with the total detected planet mass. The first planets to be found were massive ones and giants, because of the observational biases from the planet detection methods. Later, the correlation was tested for lower-mass planets, where the correlation was not observed (Udry et al. 2006; Sousa et al. 2008, 2011; Buchhave et al. 2012; Wang & Fischer 2015). Observational works for M-dwarf samples specifically have been in agreement with the correlation of giant-planet occurrence with high stellar metallicity (Bonfils et al. 2007; Johnson & Apps 2009; Schlaufman & Laughlin 2010; Rojas-Ayala et al. 2012; Terrien et al. 2012; Neves et al. 2013; Maldonado et al. 2020).

We used our planet-host M dwarfs from SWEET-Cat to examine the correlation between planetary mass and stellar metallicity. The masses of exoplanets were obtained from NASA Exoplanet Archive⁹. Altogether, 80 stars were included in our analysis: those measured for SWEET-Cat, apart from Gl699 and HIP36985 (which are not listed in the NASA Exoplanet Archive). The total number of planets orbiting those stars is 127. The low-mass planets (LMP: lower than $30 M_{\oplus}$) amount to 104, while there are 23 high-mass planets (HMP: greater than $30 M_{\oplus}$). We chose this division because the location of the gap in the distribution of planetary mass, presented in Mayor et al. (2011), is $30 M_{\oplus}$. Thus, we kept this threshold so that we could remain consistent with similar works in M dwarfs too, such as Neves et al. (2013); Maldonado et al. (2020). For systems with multiple planets, the planet with the highest mass is considered in order to characterize the star as LMP host (LMPH) or HMP host (HMPH). Our stellar sample consists of 62 LMPHs and 18 HMPHs. In Fig. 8, the mass distributions for the low-mass planets and the high-mass planets are presented. In Fig. 9 all the planetary masses in logarithmic scale are presented against the stellar host metallicities. In Fig. 10, the left panels show the relative frequencies of planets (upper left) and planet-host stars (lower left) against the metallicity distribution of stars as derived by the new version of ODUSSEAS, separated by the two planet populations. As the relative frequency, we consider the way the planets and the host stars are distributed based on the metallicity inside their own population defined by the mass division, respectively. For example, in these panels, we see that the low-mass (yellow) values of relative frequencies all sum up to 1 and the high-mass (red) values all sum up to 1 accordingly. The right panels present the absolute numbers of planets (upper right) and stars (lower right).

We notice a correlation of high-mass planets increasing at high stellar metallicity. In order to compare the distributions, we applied Kolmogorov-Smirnov tests for low-mass planets versus

high-mass planets and LMP hosts versus HMP hosts. The closer the K-S statistic number is to 0, the more likely it is that the two samples are drawn from the same distribution; whereas the closer the value is to 1, the more significant is the difference of the two samples. The p-value refers to the probability of the distributions being drawn by chance. If the p-value is very close to 0 the distributions are statistically different, while for higher p-values the distributions are similar. For the low-mass planet (LMP) versus high-mass planet (HMP) comparison we get a K-S statistic = 0.57 and a p-value = $3.09 \cdot 10^{-6}$, while for the low-mass planet host (LMPH) versus the high-mass planet host (HMPH) comparison we get a K-S statistic = 0.48 and a p-value = $1.68 \cdot 10^{-3}$. These values imply that the difference is statistically significant between the samples of low-mass planets and high-mass planets in relation to metallicity of the host stars.

Moreover, in order to examine the planetary-mass correlation regarding more stellar characteristics apart from the metallicity, we created similar distributions as before, having divided the host stars in three categories based on their T_{eff} , as indicator of their mass. In the same way, we applied Kolmogorov-Smirnov tests for each group of distributions. All the results are presented in Table 4. The numbers of planets and stars in total, as well as for each group separately, are presented in parenthesis next to each group of objects. Also, we report the average metallicity and its standard deviation for each group.

Regarding the separate groups based on T_{eff} , we notice a significant difference between the distributions of high-mass and low-mass planets around the cooler stars. In this case, the K-S statistic has the highest value of all, equal to 0.77, and the p-value is low enough, equal to 0.001; this is one order of magnitude lower than the cases of planets around intermediate and hotter stars, which have low p-values too, however (equal to 0.037 and 0.046, respectively). This clear difference in the cooler stellar range may be the outcome of a trend (as can be noticed in the lower panel of Fig. 5) indicating that the cooler metal-poor stars are measured with our new reference dataset more consistently (at least they have consistent differences from their values measured with the old reference dataset) compared to hotter metal-rich stars. The latter have more scattered differences, when comparing their values to those derived by the old reference dataset. Thus, potential systematic uncertainties in the $[\text{Fe}/\text{H}]$ values attributed to hotter stars may not make possible for equally clear differences to appear in the distributions of their planets according to stellar $[\text{Fe}/\text{H}]$. Another explanation could be that, in order to form high-mass planets at so cool stars (i.e., low masses), very high metallicity is needed to compensate.

From the comparison of distributions for our overall sample of M dwarfs and planets, the known correlation between the presence of giant planets and the high metallicity of their

⁹ <https://exoplanetarchive.ipac.caltech.edu/>

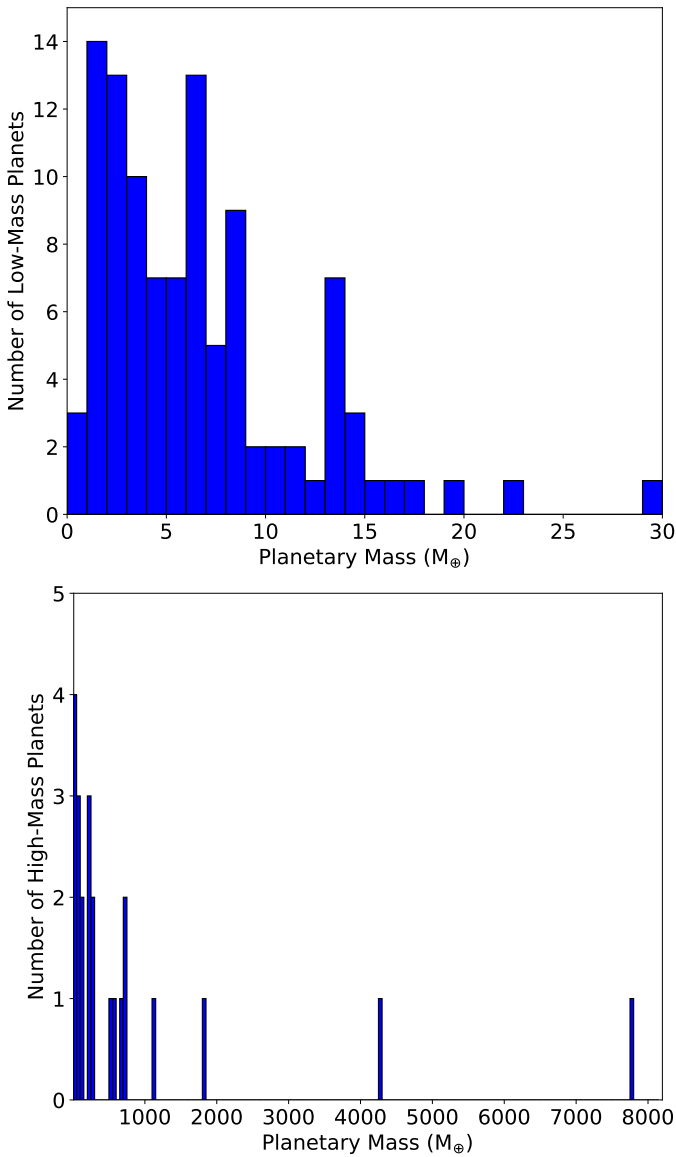


Fig. 8. Distribution of mass for the low-mass planets (upper panel). Distribution of mass for the high-mass planets (lower panel).

host stars appears to be valid in the case of M-dwarf systems as well. This result supports the core-accretion scenario (Pollack et al. 1996) against the disk-instability model (Boss 2000), as being the main mechanism of giant-planet formation around M dwarfs as well. According to Boss (2002), the formation of a giant planet as a result of disk instabilities is almost independent of the metallicity. On the other hand, the core-accretion scenario suggests that the higher the metallicity (and thus the dust density of the disk), the higher might be the probability of forming a core (and eventually massive core) before the disk dissipates (Pollack et al. 1996; Kokubo & Ida 2002). A bigger sample of M-dwarf planet hosts that have spectroscopic data available would strengthen our conclusions.

7. Summary

We present the upgraded version of our machine learning tool ODUSSEAS for the derivation of T_{eff} and $[\text{Fe}/\text{H}]$ in M dwarf stars, with spectra at wavelengths ranging between 530 and 690 nm. We explain the tests we performed with an aim to examine

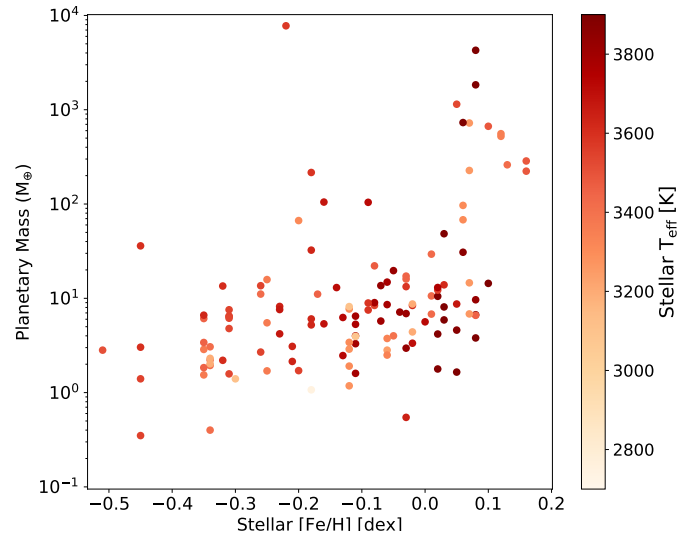


Fig. 9. Distribution in logarithmic scale of planetary masses against the host stellar metallicities.

the accuracy and precision using spectra with resolutions that vary from 190000 down to 48000. We show the results we obtained for M dwarfs in SWEET-Cat and their comparison with the old version of the tool, as well as with results from other studies in the literature.

Our new version of the tool seems to be more accurate, as its results are in agreement with several literature values within the uncertainty range. It operates with high machine learning scores of around 0.90 and achieves predictions with mean absolute errors of ~ 65 K for T_{eff} and ~ 0.04 dex for $[\text{Fe}/\text{H}]$. Taking into consideration the intrinsic uncertainties of the reference parameters, our models have maximum uncertainties of ~ 99 K for T_{eff} and ~ 0.13 dex for $[\text{Fe}/\text{H}]$, which are within the typical uncertainties for M dwarfs. Our parameters for the spectra of the same stars from different instruments have consistent values with standard deviation of ~ 30 K and ~ 0.03 dex from their average values.

We also examined the correlation between planetary mass and stellar metallicity of our sample, both as a whole and divided in groups based on T_{eff} of the stars. The presence of giant planets mostly around host stars of high metallicity appears evident for M-dwarf systems as well.

ODUSSEAS is valid for M dwarfs in the intervals 2700 to 4000 K for T_{eff} and -0.82 to 0.24 dex for $[\text{Fe}/\text{H}]$, except from very active or young stars. The spectra ought to have a S/N of above 20 for optimal predictions. The tool can be used by downloading the files from its GitHub page¹⁰, after reading the README instructions for clarifying the technical details and requirements.

Acknowledgements. This work was supported by FCT - Fundação para a Ciência e a Tecnologia through national funds and by FEDER through COMPETE2020 - Programa Operacional Competitividade e Internacionalização by these grants: UIDB/04434/2020 and UIDP/04434/2020; 2022.04416.PTDC.A.A.K., S.G.S. and E.D.M. acknowledge the support from FCT in the form of the exploratory projects with references IF/00028/2014/CP1215/CT0002, IF/00849/2015/CP1273/CT0003. S.G.S. further acknowledges the support from FCT through Investigador FCT contract nr. CEECIND/00826/2018 and POPH/FSE (EC). E.D.M. further acknowledges the support from FCT through the Stimulus FCT contract 2021.01294.CEECIND. Funded/Co-funded by the European Union (ERC, FIERCE, 101052347). Views and opinions expressed are, however, those of the authors only and do not necessarily reflect those of the European Union or the European Research Council. Neither the European Union nor the granting authority can be held responsible for them.

¹⁰ <https://github.com/AlexandrosAntoniadis/ODUSSEAS>

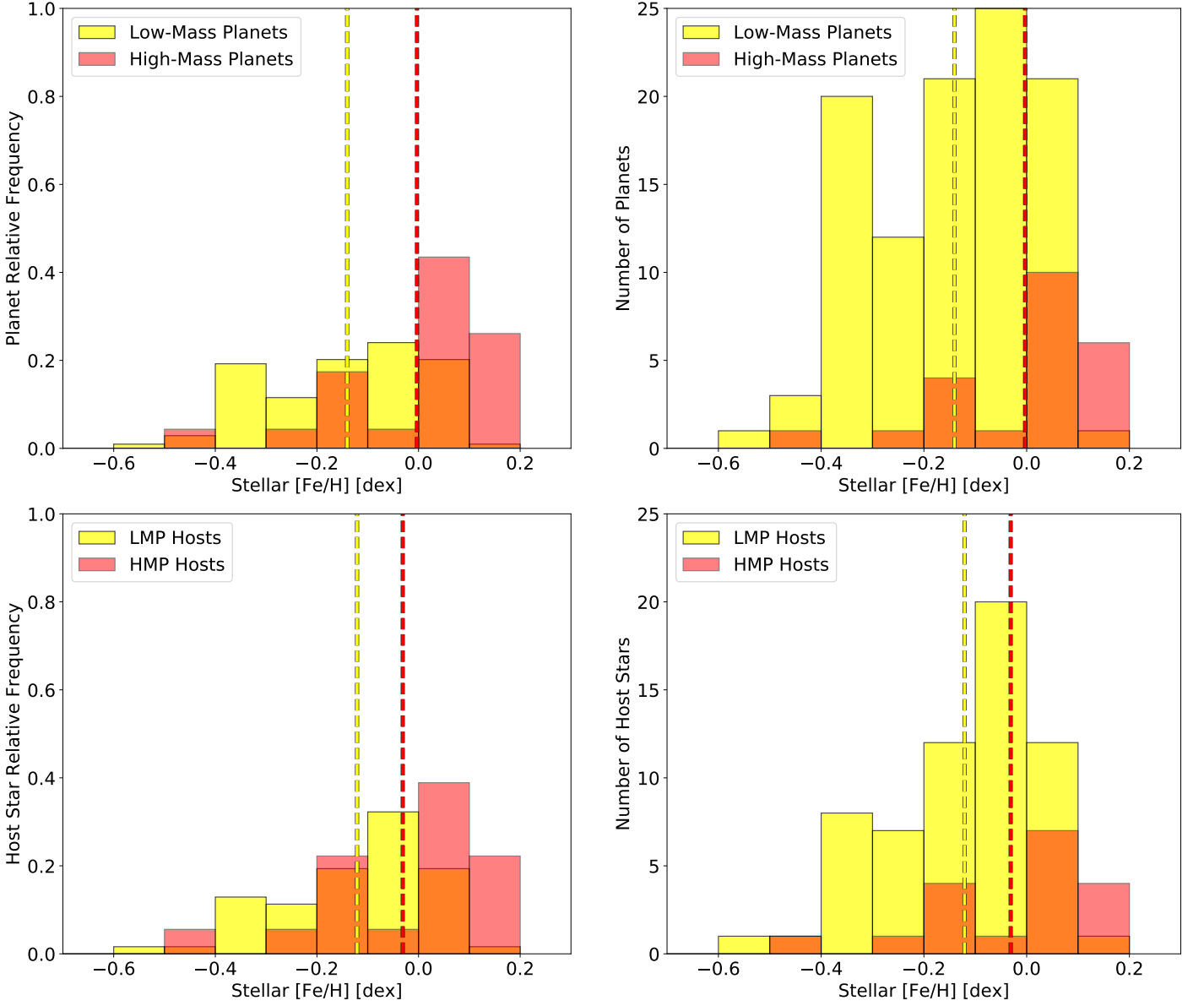


Fig. 10. Planet relative frequency distributions for the LMP and HMP populations (top-left), absolute number of planets (top-right), host star relative frequency for hosting LMP or HMP (bottom-left), and host star absolute numbers (bottom-right). The dashed lines show the mean value of stellar metallicity for each population.

Table 4. Kolmogorov–Smirnov tests comparing the LMP vs. HMP and LMPH vs. HMPH distributions for the whole sample and for different groups of stellar T_{eff} .

Samples	T_{eff} range	K-S statistic	K-S p-value	Mean [Fe/H] (St.D.)
LMP (102) vs HMP (23)	all	0.57	$3.09 \cdot 10^{-6}$	-0.14 (0.14) vs 0.00 (0.15)
LMPH (60) vs HMPH (18)	all	0.48	$1.68 \cdot 10^{-3}$	-0.12 (0.14) vs -0.03 (0.16)
LMP (24) vs HMP (7)	$T_{\text{eff}} < 3400$	0.77	$1.01 \cdot 10^{-3}$	-0.15 (0.12) vs 0.04 (0.10)
LMPH (13) vs HMPH (4)	$T_{\text{eff}} < 3400$	0.75	$3.78 \cdot 10^{-2}$	-0.16 (0.11) vs 0.01 (0.12)
LMP (49) vs HMP (10)	$3400 < T_{\text{eff}} < 3700$	0.46	$3.71 \cdot 10^{-2}$	-0.20 (0.15) vs -0.06 (0.19)
LMPH (28) vs HMPH (9)	$3400 < T_{\text{eff}} < 3700$	0.37	$2.41 \cdot 10^{-1}$	-0.17 (0.15) vs -0.08 (0.19)
LMP (29) vs HMP (6)	$T_{\text{eff}} > 3700$	0.58	$4.66 \cdot 10^{-2}$	-0.03 (0.07) vs 0.03 (0.06)
LMPH (19) vs HMPH (5)	$T_{\text{eff}} > 3700$	0.56	$1.11 \cdot 10^{-1}$	-0.03 (0.07) vs 0.03 (0.06)

Notes. In parentheses, we report the numbers of the objects for each case among the samples. We also report the mean metallicity of each sample, with the standard deviation in parentheses, respectively.

References

- Adibekyan, V. Z., Figueira, P., Santos, N. C., et al. 2013, *A&A*, 560, A51
- Akras, S., Leal-Ferreira, M. L., Guzman-Ramirez, L., & Ramos-Larios, G. 2019, *MNRAS*, 483, 5077
- Allard, F., Homeier, D., Freytag, B., et al. 2013, *Memorie della Societa Astronomica Italiana Supplementi*, 24, 128
- Antoniadis-Karnavas, A., Sousa, S. G., Delgado-Mena, E., et al. 2020, *A&A*, 636, A9
- Ball, N. M. & Brunner, R. J. 2010, *International Journal of Modern Physics D*, 19, 1049
- Bonfils, X., Delfosse, X., Udry, S., et al. 2005, *A&A*, 442, 635
- Bonfils, X., Mayor, M., Delfosse, X., et al. 2007, *A&A*, 474, 293
- Boss, A. P. 2000, *ApJ*, 536, L101
- Boss, A. P. 2002, *ApJ*, 567, L149
- Boyajian, T. S., von Braun, K., van Belle, G., et al. 2012, *ApJ*, 757, 112
- Buchhave, L. A., Latham, D. W., Johansen, A., et al. 2012, *Nature*, 486, 375
- Casagrande, L., Flynn, C., & Bessell, M. 2008, *MNRAS*, 389, 585
- Castro-González, A., Demangeon, O. D. S., Lillo-Box, J., et al. 2023, *A&A*, 675, A52
- Das, P., & Sanders, J. L. 2019, *MNRAS*, 484, 294
- Demangeon, O. D. S., Zapatero Osorio, M. R., Alibert, Y., et al. 2021, *A&A*, 653, A41
- Everett, M. E., Howell, S. B., Silva, D. R., et al. 2013, *ApJ*, 771, 107
- Fischer, D. A. & Valenti, J. 2005, *ApJ*, 622, 1102
- Gaia Collaboration 2020, *VizieR Online Data Catalog*, I/350
- Ghezzi, L., Martinez, C. F., Wilson, R. F., et al. 2021, *ApJ*, 920, 19
- Gonzalez, G., Laws, C., Tyagi, S., et al. 2001, *AJ*, 121, 432
- Hejazi, N., Lépine, S., Homeier, D., et al. 2020, *AJ*, 159, 30
- Hobson, M. J., Jordán, A., Bryant, E. M., et al. 2023, *ApJ*, 946, L4
- Howard, E. M. 2017, *Astronomical Data Analysis Software and Systems XXV*, 512, 245
- Husser, T.-O., Wende-von Berg, S., Dreizler, S., et al. 2013, *A&A*, 553, A6
- Ivezić, Ž., Connolly, A. J., VanderPlas, J. T., et al. 2014, *Statistics, Data Mining, and Machine Learning in Astronomy: A Practical Python Guide for the Analysis of Survey Data*, by Ivezić, Željko; Connolly, Andrew; Vanderplas, Jacob T.; Gray, Alexander, 2014. Princeton: Princeton University Press. OCLC: 979780267. ISBN: 9781400848911
- Johnson, J. A., & Apps, K. 2009, *ApJ*, 699, 933
- Khata, D., Mondal, S., Das, R., et al. 2021, *MNRAS*, 507, 1869
- Kokubo, E. & Ida, S. 2002, *ApJ*, 581, 666
- Laughlin, G. 2000, *ApJ*, 545, 1064
- Lépine, S., Rich, R. M., & Shara, M. M. 2007, *ApJ*, 669, 1235
- Lillo-Box, J., Figueira, P., Leleu, A., et al. 2020, *A&A*, 642, A121
- Lindgren, S., Heiter, U., & Seifahrt, A. 2016, *A&A*, 586, A100
- Loaiza-Tacuri, V., Cunha, K., Smith, V. V., et al. 2023, *ApJ*, 946, 61
- Maldonado, J., Affer, L., Micela, G., et al. 2015, *A&A*, 577, A132
- Maldonado, J., Micela, G., Baratella, M., et al. 2020, *A&A*, 644, A68
- Mann, A. W., Brewer, J. M., Gaidos, E., Lépine, S., & Hilton, E. J. 2013a, *AJ*, 145, 52
- Mann, A. W., Gaidos, E., & Ansdell, M. 2013b, *ApJ*, 779, 188
- Mann, A. W., Deacon, N. R., Gaidos, E., et al. 2014, *AJ*, 147, 160
- Mann, A. W., Feiden, G. A., Gaidos, E., et al. 2015, *ApJ*, 804, 64
- Martinez, C. F., Cunha, K., Ghezzi, L., et al. 2019, *ApJ*, 875, 29
- Mayor, M., Marmier, M., Lovis, C., et al. 2011, *arXiv:1109.2497*
- Neves, V., Bonfils, X., Santos, N. C., et al. 2012, *A&A*, 538, A25
- Neves, V., Bonfils, X., Santos, N. C., et al. 2013, *A&A*, 551, A36
- Neves, V., Bonfils, X., Santos, N. C., et al. 2014, *A&A*, 568, A121
- Newton, E. R., Charbonneau, D., Irwin, J., et al. 2015, *ApJ*, 800, 85
- Önehag, A., Heiter, U., Gustafsson, B., et al. 2012, *A&A*, 542, A33
- Passegger, V. M., Wende-von Berg, S., & Reiners, A. 2016, *A&A*, 587, A19
- Passegger, V. M., Reiners, A., Jeffers, S. V., et al. 2018, *A&A*, 615, A6
- Passegger, V. M., Schweitzer, A., Shulyak, D., et al. 2019, *A&A*, 627, A161
- Passegger, V. M., Bello-García, A., Ordieres-Meré, J., et al. 2020, *A&A*, 642, A22
- Passegger, V. M., Bello-García, A., Ordieres-Meré, J., et al. 2022, *A&A*, 658, A194
- Pepe, F., Cristiani, S., Rebolo, R., et al. 2021, *A&A*, 645, A96
- Pollack, J. B., Hubickyj, O., Bodenheimer, P., et al. 1996, *Icarus*, 124, 62
- Rabus, M., Lachaume, R., Jordán, A., et al. 2019, *MNRAS*, 484, 2674
- Rajpurohit, A. S., Allard, F., Rajpurohit, S., et al. 2018, *A&A*, 620, A180
- Rojas-Ayala, B., Covey, K. R., Muirhead, P. S., & Lloyd, J. P. 2010, *ApJ*, 720, L113
- Rojas-Ayala, B., Covey, K. R., Muirhead, P. S., & Lloyd, J. P. 2012, *ApJ*, 748, 93
- Santos, N. C., Israelian, G., Mayor, M., et al. 2003, *A&A*, 398, 363
- Santos, N. C., Israelian, G., & Mayor, M. 2004, *A&A*, 415, 1153
- Santos, N. C., Sousa, S. G., Mortier, A., et al. 2013, *A&A*, 556, A150
- Schlaufman, K. C. & Laughlin, G. 2010, *A&A*, 519, A105
- Sousa, S. G., Santos, N. C., Mayor, M., et al. 2008, *A&A*, 487, 373
- Sousa, S. G., Santos, N. C., Israelian, G., et al. 2011, *A&A*, 526, A99
- Sousa, S. G., Adibekyan, V., Delgado-Mena, E., et al. 2021, *A&A*, 656, A53
- Tabernero, H. M., Marfil, E., Montes, D., et al. 2021, *Astrophysics Source Code Library*, ascl:2111.016
- Terrien, R. C., Mahadevan, S., Bender, C. F., et al. 2012, *ApJ*, 747, L38
- Ucci, G., Ferrara, A., Gallerani, S., et al. 2019, *MNRAS*, 483, 1295
- Udry, S., Mayor, M., Benz, W., et al. 2006, *A&A*, 447, 361
- Wang, J. & Fischer, D. A. 2015, *AJ*, 149, 14
- Woolf, V. M., & Wallerstein, G. 2005, *MNRAS*, 356, 963

Appendix A: The new reference scale

Table A.1 is the new reference dataset that was added in the upgraded version of the tool. T_{eff} values of 43 stars were derived by Khata et al. (2021) and the values of the last 4 stars at the bottom were derived by Rabus et al. (2019). $[\text{Fe}/\text{H}]$ values were derived by applying the relation from Neves et al. (2012) with updated parallaxes. The intrinsic uncertainties of reference T_{eff} and $[\text{Fe}/\text{H}]$ are reported to be 99 K and 0.17 dex, respectively.

Table A.1. New reference dataset of the upgraded ODUSSEAS version.

Star	[Fe/H] [dex]	T_{eff} [K]
Gl54.1	-0.42	2900
Gl87	-0.31	3604
Gl105B	-0.14	3251
Gl176	0.00	3590
Gl179	0.13	3382
Gl203	-0.33	3227
Gl205	0.10	3813
Gl213	-0.24	3066
Gl229	-0.07	3796
Gl273	-0.07	3256
Gl299	-0.65	3246
Gl300	0.09	3106
Gl357	-0.28	3395
Gl382	0.01	3672
Gl393	-0.14	3569
Gl402	0.02	3077
Gl436	-0.04	3401
Gl465	-0.56	3571
Gl480.1	-0.54	3373
Gl486	-0.01	3329
Gl514	-0.15	3671
Gl526	-0.15	3664
Gl536	-0.12	3674
Gl555	0.13	3258
Gl581	-0.20	3344
Gl628	-0.06	3362
Gl643	-0.32	3243
Gl678.1A	-0.05	3704
Gl686	-0.30	3670
Gl699	-0.61	3256
Gl701	-0.22	3646
Gl752A	0.02	3538
Gl846	-0.07	3810
Gl849	0.19	3516
Gl876	0.13	3202
Gl880	0.03	3703
Gl908	-0.40	3475
Gl1125	-0.15	3328
Gl1129	0.00	3112
Gl1256	-0.05	2992
Gl1265	-0.21	3045
Gl2066	-0.12	3597
LP816-60	-0.11	3071
Gl1	-0.42	3616
Gl674	-0.19	3409
Gl832	-0.21	3512
Gl887	-0.29	3692

Appendix B: The determinations for 82 stars in SWEET-Cat

Table B.1 contains the derived parameters with their maximum uncertainties, applying both the new and the old reference datasets. For stars with spectra from multiple instruments, we present all our measurements.

Table B.1. Determinations for the parameters and total error budgets for 82 stars in SWEET-Cat with the new and the old reference datasets.

Star	Spec.	T_{eff} (New) [K]	[Fe/H] (New) [dex]	T_{eff} (Old) [K]	[Fe/H] (Old) [dex]
CD Cet	CARMENES	3091±115	-0.11±0.13	3113±98	-0.23±0.14
G264-012	CARMENES	3339±104	-0.06±0.13	3237±87	-0.12±0.13
G115A	HARPS-N	3602±91	-0.45±0.11	3546±65	-0.39±0.10
G115A	CARMENES	3656±107	-0.33±0.13	3604±83	-0.29±0.12
G115A	SOPHIE	3602±100	-0.33±0.13	3484±78	-0.30±0.13
G127.1	HARPS	3715±90	-0.14±0.11	3566±66	-0.09±0.10
G127.1	UVES	3713±94	-0.11±0.11	3597±69	-0.08±0.10
G127.1	FEROS	3703±107	-0.07±0.13	3622±87	-0.06±0.13
G149	HARPS-N	3726±91	0.00±0.11	3485±65	0.04±0.10
G149	CARMENES	3670±100	0.03±0.12	3522±79	0.02±0.12
G149	SOPHIE	3788±102	0.02±0.13	3438±80	0.12±0.13
G196	CARMENES	3821±100	-0.05±0.12	3680±80	-0.04±0.13
G196	SOPHIE	3830±100	0.00±0.13	3656±80	-0.01±0.13
G1163	HARPS	3431±93	0.01±0.11	3217±65	0.01±0.10
G1163	FEROS	3507±108	0.03±0.13	3275±85	0.02±0.13
G1176	HARPS	3623±90	-0.02±0.11	3390±65	0.01±0.10
G1176	CARMENES	3426±109	-0.04±0.13	3389±90	-0.13±0.13
G1176	SOPHIE	3628±102	-0.03±0.13	3382±80	0.05±0.13
G1179	CARMENES	3420±103	0.13±0.12	3263±81	0.02±0.13
G1179	SOPHIE	3405±108	0.10±0.14	3140±81	0.08±0.13
G1179	FEROS	3386±116	0.06±0.13	3188±90	0.07±0.13
G1180	HARPS	3544±90	-0.31±0.11	3423±65	-0.26±0.10
G1180	UVES	3580±95	-0.28±0.11	3485±71	-0.28±0.10
G1180	CARMENES	3567±101	-0.31±0.12	3501±80	-0.27±0.12
G1180	FEROS	3585±105	-0.24±0.13	3474±85	-0.21±0.13
G1229	HARPS	3782±90	-0.06±0.11	3577±65	-0.01±0.10
G1229	ESPRESSO	3751±92	-0.05±0.11	3555±66	-0.02±0.10
G1229	UVES	3801±97	-0.02±0.11	3622±71	-0.04±0.10
G1229	CARMENES	3738±101	-0.07±0.13	3605±79	-0.05±0.12
G1251	SOPHIE	3397±100	-0.05±0.13	3221±79	-0.07±0.13
G1273	HARPS	3282±92	-0.12±0.11	3103±65	-0.09±0.10
G1273	HARPS-N	3297±93	-0.15±0.11	3120±66	-0.13±0.10
G1273	CARMENES	3237±107	-0.19±0.13	3188±83	-0.14±0.12
G1273	SOPHIE	3244±103	-0.03±0.13	3153±80	-0.08±0.13
G1273	FEROS	3344±137	-0.20±0.14	3219±96	-0.17±0.14
G1317	HARPS	3354±94	0.12±0.11	3143±66	0.14±0.10
G1317	FEROS	3497±122	0.12±0.14	3232±92	0.12±0.14
G1328	UVES	3925±98	0.06±0.11	3854±73	-0.01±0.11
G1328	SOPHIE	3929±106	0.10±0.14	3829±84	-0.01±0.14
G1328	FEROS	3924±112	0.15±0.14	3876±87	-0.01±0.14
G1357	HARPS	3458±90	-0.35±0.11	3342±65	-0.30±0.10
G1357	HARPS-N	3473±94	-0.37±0.11	3388±67	-0.34±0.10
G1357	UVES	3474±94	-0.29±0.11	3400±70	-0.27±0.10
G1357	FEROS	3532±129	-0.26±0.14	3426±100	-0.24±0.14
G1367	FEROS	3651±108	-0.03±0.13	3424±86	-0.03±0.13
G1378	SOPHIE	3758±101	0.02±0.13	3613±80	-0.01±0.13
G1393	HARPS	3549±92	-0.20±0.11	3411±65	-0.17±0.10
G1393	ESPRESSO	3530±92	-0.22±0.11	3425±65	-0.19±0.10
G1393	CARMENES	3561±102	-0.18±0.12	3501±80	-0.19±0.12
G1393	SOPHIE	3500±101	-0.13±0.13	3419±80	-0.15±0.13
G1393	FEROS	3628±106	-0.15±0.13	3462±87	-0.16±0.13
G1422	HARPS	3459±95	-0.17±0.11	3259±66	-0.16±0.10
G1422	UVES	3458±102	-0.18±0.11	3308±73	-0.20±0.11
G1422	FEROS	3527±118	-0.15±0.13	3317±88	-0.15±0.14
G1433	HARPS	3630±90	-0.18±0.11	3468±65	-0.14±0.10
G1433	UVES	3637±94	-0.19±0.11	3521±67	-0.19±0.10

Table B.1. continued

Star	Spec.	T_{eff} (New) [K]	[Fe/H] (New) [dex]	T_{eff} (Old) [K]	[Fe/H] (Old) [dex]
Gl436	HARPS	3478±91	-0.08±0.11	3289±65	-0.04±0.10
Gl436	HARPS-N	3458±96	-0.13±0.11	3326±67	-0.12±0.10
Gl436	CARMENES	3476±103	-0.03±0.12	3418±84	-0.09±0.12
Gl436	SOPHIE	3422±100	-0.01±0.13	3318±80	-0.04±0.13
Gl436	FEROS	3531±107	-0.01±0.13	3347±84	-0.04±0.13
Gl463	HARPS-N	3532±95	0.05±0.11	3324±66	0.05±0.10
Gl463	CARMENES	3582±109	0.02±0.13	3505±91	-0.05±0.13
Gl463	SOPHIE	3577±132	0.04±0.14	3339±96	0.06±0.14
Gl486	HARPS	3246±93	-0.06±0.11	3105±68	-0.06±0.10
Gl486	ESPRESSO	3231±112	0.06±0.13	3151±77	0.01±0.13
Gl486	UVES	3340±97	-0.06±0.11	3183±71	-0.06±0.11
Gl486	FEROS	3395±107	-0.01±0.13	3173±85	-0.06±0.13
Gl536	HARPS	3694±90	-0.16±0.11	3559±65	-0.13±0.10
Gl536	HARPS-N	3707±90	-0.16±0.11	3583±65	-0.16±0.10
Gl536	CARMENES	3698±104	-0.14±0.12	3634±80	-0.17±0.12
Gl536	FEROS	3706±124	-0.10±0.14	3581±89	-0.11±0.14
Gl581	HARPS	3367±91	-0.25±0.11	3224±65	-0.21±0.10
Gl581	CARMENES	3426±100	-0.20±0.12	3359±85	-0.19±0.12
Gl581	FEROS	3468±115	-0.17±0.13	3305±90	-0.21±0.14
Gl625	HARPS-N	3509±92	-0.51±0.11	3459±66	-0.47±0.10
Gl625	CARMENES	3530±106	-0.45±0.12	3487±80	-0.42±0.12
Gl625	SOPHIE	3548±102	-0.41±0.13	3419±84	-0.36±0.13
Gl649	HARPS	3720±90	-0.09±0.11	3546±65	-0.04±0.10
Gl649	CARMENES	3671±102	-0.06±0.12	3577±69	-0.06±0.12
Gl649	SOPHIE	3708±100	-0.05±0.13	3512±80	-0.04±0.13
Gl674	HARPS	3425±91	-0.26±0.11	3304±65	-0.22±0.10
Gl674	ESPRESSO	3417±92	-0.29±0.11	3292±66	-0.24±0.10
Gl674	FEROS	3484±108	-0.16±0.13	3344±84	-0.17±0.13
Gl676A	HARPS	3978±92	0.08±0.11	3732±67	0.08±0.11
Gl676A	FEROS	3982±114	0.12±0.14	3775±88	0.08±0.14
Gl680	HARPS	3572±90	-0.22±0.11	3431±65	-0.17±0.10
Gl680	FEROS	3603±109	-0.24±0.13	3473±87	-0.13±0.14
Gl682	UVES	3202±101	-0.02±0.11	3108±73	-0.06±0.10
Gl682	ESPRESSO	3232±106	0.08±0.12	3102±74	0.05±0.11
Gl682	FEROS	3324±112	0.01±0.14	3100±92	0.01±0.14
Gl685	HARPS-N	3787±91	-0.08±0.11	3635±65	-0.04±0.10
Gl685	CARMENES	3721±103	-0.05±0.12	3642±80	-0.04±0.12
Gl685	SOPHIE	3754±101	-0.05±0.13	3614±81	-0.01±0.13
Gl686	HARPS	3632±91	-0.35±0.11	3566±65	-0.31±0.10
Gl686	CARMENES	3633±103	-0.26±0.13	3563±82	-0.29±0.13
Gl686	SOPHIE	3657±101	-0.28±0.13	3577±79	-0.27±0.13
Gl686	FEROS	3652±108	-0.22±0.13	3612±88	-0.24±0.14
Gl687	HARPS-N	3453±94	-0.03±0.11	3273±66	-0.03±0.10
Gl687	SOPHIE	3453±104	0.03±0.13	3288±82	0.00±0.13
Gl699	HARPS	3226±91	-0.62±0.11	3113±68	-0.58±0.10
Gl699	HARPS-N	3258±93	-0.62±0.11	3160±68	-0.59±0.10
Gl699	UVES	3300±97	-0.57±0.11	3191±75	-0.56±0.11
Gl699	CARMENES	3228±114	-0.53±0.13	3161±87	-0.58±0.13
Gl699	SOPHIE	3199±103	-0.52±0.13	3161±82	-0.53±0.13
Gl720A	HARPS-N	3832±92	-0.07±0.11	3759±66	-0.12±0.10
Gl720A	CARMENES	3778±106	-0.06±0.13	3773±81	-0.12±0.13
Gl720A	SOPHIE	3774±103	0.05±0.13	3716±81	-0.04±0.13
Gl740	HARPS	3832±91	-0.04±0.11	3663±66	-0.02±0.10
Gl740	HARPS-N	3837±91	-0.06±0.11	3691±66	-0.04±0.10
Gl740	CARMENES	3779±103	-0.01±0.13	3721±82	-0.05±0.13
Gl740	SOPHIE	3824±102	-0.02±0.13	3717±84	-0.05±0.13
Gl740	FEROS	3808±102	0.02±0.13	3673±82	-0.01±0.13

Table B.1. continued

Star	Spec.	T_{eff} (New) [K]	[Fe/H] (New) [dex]	T_{eff} (Old) [K]	[Fe/H] (Old) [dex]
Gl752A	HARPS	3554±91	0.02±0.11	3337±65	0.05±0.10
Gl752A	CARMENES	3540±100	0.01±0.12	3384±78	0.02±0.12
Gl752A	SOPHIE	3580±99	0.09±0.13	3349±80	0.05±0.13
Gl832	HARPS	3587±90	-0.18±0.11	3459±65	-0.14±0.10
Gl832	FEROS	3563±103	-0.11±0.13	3466±82	-0.11±0.13
Gl849	HARPS	3486±95	0.16±0.11	3208±66	0.20±0.10
Gl849	CARMENES	3471±106	0.20±0.12	3333±89	0.12±0.12
Gl876	FEROS	3265±108	0.07±0.13	3102±84	0.08±0.13
Gl887	HARPS	3679±90	-0.23±0.11	3578±65	-0.19±0.10
Gl887	FEROS	3701±112	-0.17±0.14	3584±84	-0.14±0.13
Gl1214	UVES	3109±129	-0.12±0.12	3005±80	-0.06±0.12
Gl1214	FEROS	3115±129	-0.04±0.14	3022±95	-0.09±0.14
Gl3082	HARPS	3645±90	-0.23±0.11	3508±65	-0.18±0.10
Gl3082	UVES	3674±95	-0.19±0.11	3570±69	-0.17±0.10
Gl3082	FEROS	3681±108	-0.14±0.13	3550±83	-0.12±0.13
Gl3090	HARPS	3701±91	-0.02±0.11	3509±67	0.01±0.10
Gl3090	FEROS	3737±104	0.04±0.13	3536±83	0.02±0.13
Gl3138	HARPS	3884±92	0.02±0.11	3797±69	-0.05±0.11
Gl3323	FEROS	3195±114	-0.34±0.14	3092±89	-0.33±0.14
Gl3341	HARPS	3455±100	0.08±0.12	3433±74	-0.02±0.12
Gl3470	UVES	3620±106	0.03±0.11	3385±76	0.09±0.11
Gl3634	HARPS	3535±92	-0.08±0.11	3347±65	-0.02±0.10
Gl3942	HARPS-N	3823±90	-0.04±0.11	3680±66	-0.04±0.10
Gl3998	HARPS	3729±91	-0.13±0.11	3557±65	-0.09±0.10
Gl3998	HARPS-N	3720±91	-0.13±0.11	3557±65	-0.07±0.10
Gl3998	FEROS	3712±102	-0.03±0.13	3546±83	-0.03±0.13
Gl9066	CARMENES	3317±114	-0.20±0.13	3232±102	-0.35±0.14
Gl9689	HARPS	3832±94	0.08±0.11	3674±66	0.05±0.10
Gl9689	HARPS-N	3850±94	0.01±0.11	3692±66	0.00±0.10
HD238090	CARMENES	3812±107	-0.03±0.13	3800±83	-0.11±0.13
HD260655	ESPRESSO	3639±103	-0.21±0.12	3632±69	-0.22±0.11
HD260655	CARMENES	3671±116	-0.21±0.14	3750±82	-0.28±0.13
HIP4845	HARPS	3915±98	0.10±0.12	3900±76	-0.06±0.13
HIP36985	HARPS	3809±95	-0.01±0.11	3634±72	-0.01±0.11
HIP36985	CARMENES	3800±105	0.03±0.13	3667±87	-0.05±0.13
HIP36985	FEROS	3834±110	0.05±0.14	3643±93	0.01±0.14
HIP38594	HARPS	3903±97	0.03±0.11	3874±72	-0.10±0.12
HIP57050	CARMENES	3305±102	0.06±0.12	3161±80	0.02±0.12
HIP57050	SOPHIE	3348±104	0.03±0.13	3134±82	0.01±0.13
HIP79431	FEROS	3488±124	0.10±0.13	3281±89	0.20±0.13
K2-3	HARPS	3788±96	-0.11±0.12	3815±69	-0.19±0.11
K2-3	HARPS-N	3752±96	-0.09±0.12	3773±70	-0.16±0.11
K2-3	FEROS	3748±117	-0.04±0.14	3836±94	-0.16±0.14
K2-18	CARMENES	3587±113	-0.09±0.13	3534±112	-0.19±0.15
K2-122	HARPS-N	3906±94	0.05±0.11	3668±66	0.03±0.10
L98-59	HARPS	3420±92	-0.34±0.11	3297±66	-0.31±0.10
L168-9	HARPS	3872±91	0.05±0.11	3634±65	0.06±0.10
L168-9	FEROS	3842±103	0.11±0.13	3645±84	0.10±0.13
Lalande21185	UVES	3529±115	-0.26±0.12	3467±76	-0.23±0.11
Lalande21185	CARMENES	3518±121	-0.32±0.12	3557±81	-0.35±0.12
LHS1678	HARPS	3549±94	-0.45±0.11	3456±65	-0.42±0.10
LHS1815	HARPS	3678±92	0.05±0.11	3458±66	0.05±0.10
LP714-47	ESPRESSO	3860±92	0.06±0.11	3606±66	0.08±0.10
LSPMJ2116+0234	FEROS	3590±108	-0.03±0.13	3302±86	-0.01±0.13
LTT1445A	HARPS	3374±92	-0.36±0.11	3240±68	-0.35±0.10
LTT1445A	ESPRESSO	3330±92	-0.42±0.11	3242±68	-0.39±0.10
Proxima Centauri	HARPS	2756±112	-0.18±0.11	2702±69	-0.12±0.10

Table B.1. continued

Star	Spec.	T_{eff} (New) [K]	[Fe/H] (New) [dex]	T_{eff} (Old) [K]	[Fe/H] (Old) [dex]
Proxima Centauri	UVES	2804±113	-0.21±0.11	2833±78	-0.23±0.11
Ross128	HARPS	3114±93	-0.30±0.11	2983±66	-0.26±0.10
Ross128	FEROS	3166±111	-0.30±0.13	3085±90	-0.28±0.14
TOI-270	HARPS	3539±92	-0.31±0.11	3422±66	-0.29±0.10
TOI-270	ESPRESSO	3465±93	-0.38±0.11	3407±66	-0.33±0.10
TOI-776	HARPS	3765±90	-0.11±0.11	3634±66	-0.10±0.10
TOI-776	ESPRESSO	3730±91	-0.13±0.11	3621±66	-0.12±0.10
TOI-1235	HARPS-N	3925±94	0.03±0.11	3824±68	-0.04±0.11
TOI-1266	HARPS-N	3614±92	-0.32±0.11	3521±66	-0.28±0.10
TOI-1801	HARPS-N	3797±91	-0.07±0.11	3698±69	-0.09±0.11
TYC-2187-512-1	CARMENES	3682±102	-0.16±0.13	3620±80	-0.14±0.13
TYC-2187-512-1	FEROS	3678±105	-0.16±0.13	3615±84	-0.14±0.13
Wolf1061	HARPS	3307±92	-0.12±0.11	3103±66	-0.08±0.10
Wolf1061	CARMENES	3315±100	-0.03±0.12	3211±81	-0.07±0.12
Wolf1061	FEROS	3357±132	-0.10±0.14	3207±99	-0.10±0.14